Title

Enzymatic Syntheses and Applications of Fluorescent Cyclic Dinucleotides

Journal

Chemistry - A European Journal, 26(27)

ISSN

0947-6539

Authors

Li, Yao

Ludford, Paul T

Fin, Andrea

et al.

Publication Date

2020-05-12

DOI

10.1002/chem.202001194

Peer reviewed

Published in final edited form as:

Chemistry. 2020 May 12; 26(27): 6076–6084. doi:10.1002/chem.202001194.

Enzymatic Syntheses and Applications of Fluorescent Cyclic Dinucleotides

Yao Li[a], **Paul T. Ludford III**[a], **Andrea Fin**[a],[b], **Alexander R. Rovira**[a], **Yitzhak Tor**[a]

[a]Department of Chemistry and Biochemistry, University of California San Diego, 9500 Gilman Drive, La Jolla, CA 92093-0358, USA

[b]Dipartimento di Scienza e Tecnologia del Farmaco, University of Turin, Via P. Giuria 9, 10125 Turin, Italy

Abstract

Bacterial cyclic dinucleotides (CDNs) play important roles in regulating biofilm formation, motility and virulence. In eukaryotic cells, theses bacterial CDNs are recognized as pathogen-associated molecular patterns (PAMPs) and trigger an innate immune response. We report the photophysical analyses of a novel group of enzymatically synthesized emissive CDN analogues comprised of two families of isomorphic ribonucleotides. The highly favorable photophysical features of the CDN analogues, when compared to their non-emissive natural counterparts, are used to monitor in real time the dinucleotide cyclase-mediated synthesis and phosphodiesterase (PDE)-mediated hydrolysis of homodimeric and mixed CDNs, providing effective means to probe the activities of two classes of bacterial enzymes and insight into their biomolecular recognition and catalytic features.

Graphical Abstract

ytor@ucsd.edu.

Supporting information for this article is given via a link at the end of the document

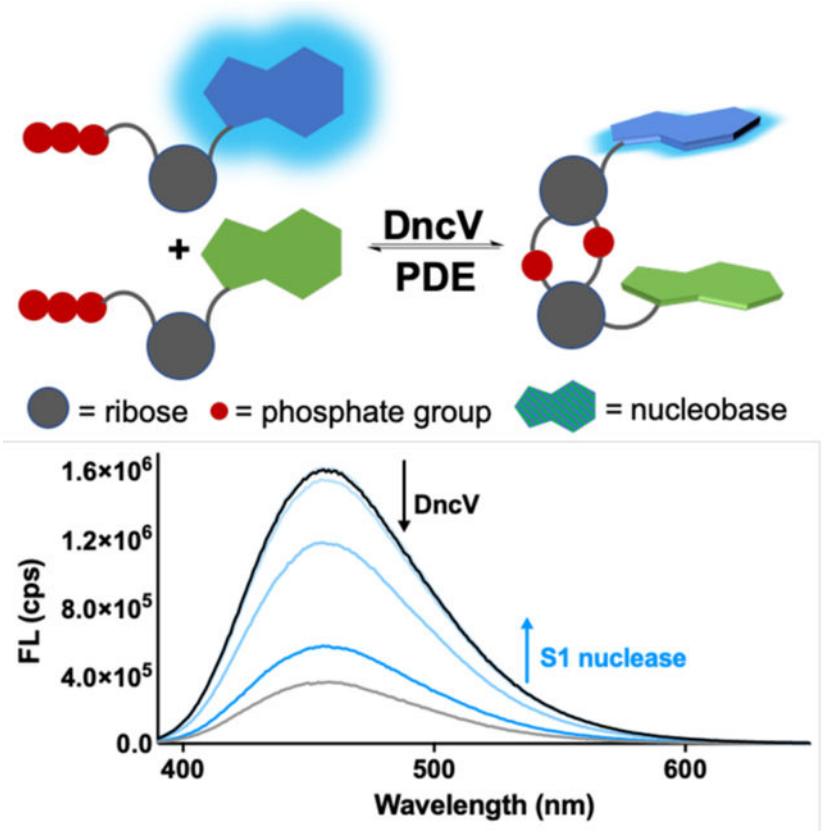

CDNs are second messengers that regulate central processes in all bacteria. The enzymatic syntheses and applications of novel isomorphic fluorescent CDN analogues are reported, illustrating their utility in probing the activities of two classes of bacterial enzymes and providing insight into their biomolecular recognition and catalytic features.

Keywords

Cyclic dinucleotides; fluorescence; enzyme kinetics; DncV; rocR

Introduction

Cyclic dinucleotides (CDNs) are second messengers that regulate central processes in all bacteria, including biofilm formation, motility and virulence.[1] The most studied derivatives include the purine-containing c-di-GMP, c-di-AMP and 3',3'-c-GAMP.[2] The recent discovery of c-di-UAMP in *E. coli* suggests, however, that pyrimidine nucleotides can also be engaged in forming CDNs in vivo.[3] Bacterial CDNs are recognized as pathogen-associated molecular patterns (PAMPs) and trigger the innate immune response in eukaryotic cells.[2–3, 4] As their regulatory roles are gradually being recognized,[1a, 5] analogues that can shed light on the pathways involved in their production, degradation and recognition are of significance.

CDNs are produced from two nucleotide triphosphates (NTPs) by dinucleotide cyclases. GGDEF and DisA domains are responsible for the synthesis of c-di-GMP and c-di-AMP. DncV, cGAS and the recently discovered cdnE are able to produce the heterodimeric CDNs, 3',3'-c-GAMP, 2',3'-c-GAMP and 3',3'-c-UAMP, respectively.[6] Whereas cGAS or cdnE have not been shown to generate any homodimeric CDNs, DncV was reported to be promiscuous and produce c-di-GMP and, c-di-AMP, in addition to 3',3'-c-GAMP, when provided with purine nucleotides *in vitro*.[7]

The global and local concentrations of bacterial CDNs are tightly regulated in response to intracellular and extracellular signals.[1a, 8] This control is achieved by the orchestrated activity of dinucleotide cyclases and phosphodiesterases (PDEs), which cleave CDNs into either linear pNpNs or monomeric nucleotides.[5b] For example, PDEs containing EAL domains, (i.e. rocR from *P. aeruginosa)* hydrolyze c-di-GMP into pGpG while those with HD-GYP domain cleaves it into GMP. [1a, 2]

Interrogating the *in vitro* syntheses and hydrolyses of CDNs often relies on chromatographic techniques. While reliable and informative, such tools are not amenable to real-time monitoring and high throughput analyses, a feature frequently afforded by fluorescence-based methods. Applying the latter is challenging, however, as the natives CDNs are non-emissive and modifications aimed at conferring favorable photophysical features might perturb the processes of interest. Indeed, while using synthetic CDNs containing common emissive nucleosides to fluorescently monitor PDE-mediated c-di-GMP degradation and hydrolysis has been demonstrated (using 2-aminopurine),[9] applying such strategies to the study of dinucleotide cyclases demands higher isomorphicity and substrate recognition of the NTP precursors, criteria not regularly found among common emissive nucleoside analogues.[10]

Recent efforts in our laboratory have yielded two families of isomorphic emissive ribonucleosides, the thiopheno- and isothiazolo-based RNA alphabets (thN and ^{tz}N, respectively; see examples in Figure 1).[11] The two families display distinctive photophysical properties and have been used to investigate catalytic RNAs, nucleoside metabolizing enzymes and diverse nucleotide-based cofactors.[12] We surmised that the isomorphic fluorescent purines analogues' visible emission and sensitivity to environmental changes could be exploited to study the enzymes involved in CDNs biosynthesis and degradation, as schematically illustrated in Figure 1.

While polymorphic, prone to aggregation and highly dependent on conditions, c-di-GMP displays stacking of the two nucleobases in solution.[13] This suggests distinct photophysics for any CDN compared to that displayed by its precursors (NTPs) or degraded products (pN or pNpN). We further hypothesized that when thGTP or ^{tz}GTP would cyclize to the corresponding CDNs, the fluorescence would likely diminish and, conversely, phosphodiester hydrolysis of emissive CDNs would lead to fluorescence enhancement (Figure 1). Such signal change can thus be used to monitor the process in real-time, determine reaction kinetics and, in principle, be used to facilitate inhibitor discovery. Herein we report the fluorescence-based monitoring of CDN synthesis and hydrolysis using **thG** and **^{tz}G**, two isomorphic guanosine surrogates. The resulting structure-activity relationship

provides insight into the substrate recognition and catalytic mechanisms of the CDN-specific PDEs studied.

Results and Discussion

Enzymatic synthesis of c-di-GMP analogues with DncV.

CDN analogues have greatly facilitated mechanistic, biochemical and structural studies, particularly in the context of CDN-binding riboswitches and protein receptors.[7b, 9, 14] The biggest hindrance to such studies has frequently been the preparation of analogues, as they have been predominately stepwise synthesized using phosphoramidite chemistry.[7b, 15] We employed DncV, a cyclic dinucleotide synthetase from *Vibrio cholerae*, to enzymatically produce a series of c-di-GMP analogues. While this enzyme primarily synthesizes 3',5-'c-GAMP *in vivo*, when provided with only GTP or ATP *in vitro* it is also capable of making c-di-GMP and c-di-AMP.[16] Since DncV can accept both guanosine and adenosine, we postulated it would tolerate the thiopheno and isothiazolo G surrogates, members of our previously synthesized emissive RNA alphabets (Figure 1).[11]

To benchmark the enzymatic synthesis of c-di-GMP and the corresponding emissive analogues, DncV was incubated with GTP, thGTP and ^{tz}GTP (Figure 2). The reactions were analyzed by HPLC and mass spectrometry (Figure 3, S1–S4). After 40 minutes of incubation with 500 μM GTP, ^{tz}GTP or thGTP at 37 °C, c-di-GMP, c-di-^{tz}GMP and c-di-thGMP were obtained in 94%, 81% and 11% yields, respectively. DncV also produced the mixed c-G^{tz}GMP when incubated with 500 μM each of GTP and ^{tz}GTP (Figure S5a). When incubated with a mixture of 500 μM of GTP and thGTP, DncV also produces all three plausible products c-diGMP, c-GthGMP and c-di-thGMP (Figure S5b). Based on HPLC analyses shown in Figure 3, the overall yields of c-di-GMP (40 mins), c-di-^{tz}GMP (80 mins), and c-di-thGMP (300 mins) were 94%, 85% and 62%, respectively. These results have indeed confirmed the tolerance level of DncV to thGTP and ^{tz}GTP, our emissive NTPs. Both symmetric and mixed CDN analogues were successfully synthesized in this fashion (Figure 2).

DncV generates CDNs through a series of sequential reactions, which are thought to involve a release-and-rebound process of the intermediate.[7b, 17] After the first 3',5'-phosphordiester bond formation, the linear dinucleotide pppNpN is released and oppositely rebound to the enzyme, after which the second 3',5'-phosphodiester linkage is made.[7b, 16b, 18] To ultimately apply and interpret real-time fluorescence measurements, a better understanding of the enzymatic conversion of GTP and its analogues into the corresponding CDNs is therefore required. The reaction time course was consequently analyzed, paying particular attention to the accumulation and consumption of intermediates. DncV was incubated with GTP, ^{tz}GTP and thGTP, and the reactions containing each of the corresponding substrates were quenched with calf intestinal alkaline phosphatase (CIAP) at designated time points.[19] The relative concentrations of the starting material (S), uncyclized intermediate (I) and product (P) were then monitored by HPLC. The integrated area under the peak for each species was corrected using the corresponding extinction coefficient (Methods and Supporting experiments sections in SI) and normalized to its relative concentration, which were then plotted against time. Taking into account the unique

release-andrebound process of the uncyclized dinucleotide intermediate,[16b, 20] the kinetics of the DncV-mediated CDN syntheses was therefore analyzed according to the model in Scheme 1a and the differential equations (Eq 1–4), where S represents the starting NTP, I_1 and I_2 respectively represent intermediates pppNpN and degraded intermediate pNpN (I= I_1 + I_2), and P represents the product CDN:

$$d[S]/dt = -2k_1[S]^2 \quad (1)$$

$$d[I_1]/dt = k_1[S]^2 - k_2[1/1] - k_3[I_1] \quad (2)$$

$$d[P]/dt = k_2[I_1] \quad (3)$$

$$d[I_2]/dt = k_3[I_1] \quad (4)$$

A small amount of uncyclized intermediate was observed during the synthesis of c-di-GMP (Figure 3a–c), and the calculated k_1, k_2 and k_3 values were found to be (7.1±2.3)×10^{-6} μM $^{-1}s^{-1}$, (7.4±2.1)×10^{-2} and (6.4±0.3)×10^{-4} s^{-1}, respectively (Table 1). When incubated with ^{tz}GTP, a larger amount of the intermediate was accumulated in the first 10 minutes resulting in an S-shaped product formation curve (Figure 3d–f).[21] The calculated k_1, k_2 and k_3 values were (1.26±0.07)×10^{-6} $\mu M^{-1}s^{-1}$, (3.4±0.2)×10^{-3} and (1.3±0.1)×10^{-4} s^{-1}, respectively. DncV was also found to convert thGTP into the corresponding c-di-thGMP with k_1, k_2 and k_3 values of (3.08±0.03)×10^{-7} $\mu M^{-1}s^{-1}$, (2.32±0.05)×10^{-4} and (2.91±0.01) ×10^{-5} s^{-1}, respectively (Figure 3g–i). After 5 h of incubation, 62% of thGTP was converted to c-di-thGMP. Obvious accumulation of the reaction intermediate is seen for the first 80 minutes (Figure 3g, 3i). The relatively fast degradation of the intermediate compared to product formation (k_2/k_3 was calculated to be 8.0 for c-di-thGMP synthesis, compared to 26 for c-di-^{tz}GMP and 116 for c-di-GMP) resulted in relatively high concentration (13% after 300 min) of persistent uncyclized intermediates (Figure 3i).done in duplicates. Error bars indicate standard deviation (SD).

The guanosine surrogates used here illuminate the key functional elements in the purine scaffold that affect the formation and consumption of the reaction intermediate. The kinetic constants listed in Table 1 illustrate that the formation of the first phosphodiester linkage is the rate-limiting step for the syntheses of c-di-GMP, c-di-^{tz}GMP and c-di-thGMP.[22] Furthermore, a certain fraction of the uncyclized intermediate is not entirely consumed in all three reactions (Figure 3c, 3f, 3i). We speculate that the hydrolysis of the open intermediate pppNpN (I_1 in Scheme 1a) to the unreactive pNpN (I_2 in Scheme 1a) could take place.[23] Additionally, the consumption of thGTP in c-di-thGMP synthesis was observed to be slower than calculated. We speculate that this might be caused by a non-productive DncV-mediated hydrolysis of thGTP to thG monophosphate (pthG), circumventing the formation of the inter-nucleotide phosphodiester bond. Our findings support the hypothesis that the absence of the purine's N-7 can alter the reaction kinetics, although previous structural studies with DncV have not revealed a direct contact between N-7 of GTP and any protein residues.[16b, 18, 20].

Photophysical properties of emissive c-di-GMP analogues.

Steady state absorption and emission measurements show hypsochromic shifts in the absorption maxima of thG and ^{tz}G upon incorporation into the corresponding cyclic dinucleotides (Figure 4, Table 2). While relatively small (< 10 nm), this trend is suggestive of multichromophoric arrangements reminiscent of Haggregates.[24] The emission energy of the thG- and ^{tz}G-containing CDNs remains relatively close to that of the parent nucleosides and, intriguingly, the thG-containing derivatives still display the high energy shoulder associated with its tautomeric forms.[25] Comparing the emission quantum yields (Φ) of the fluorescent CDNs to those of the monomeric nucleosides show significant quenching of the former, as predicted (Table 2). Interestingly, thG exhibits a significantly enhanced self-quenching effect relative to guanosine; the emission quantum yield values for c-di-thGMP and c-GthGMP were about 17% and 39% of Φ^{th}_{G}, respectively. The self-quenching effect of ^{tz}G resulted in the low quantum yield for c-di-^{tz}GMP (16% of Φ^{tz}_{G}), which is comparable to that seen for c-G^{tz}GMP (19% of Φ^{tz}_{G}). These results match the model illustrated in Figure 1, where decreased emission intensity was expected upon the conversion of the emissive NTPs into CDNs. Further analysis below provides additional insight into this model and its potential applications.

Monitoring DncV-mediated synthesis of c-di-GMP analogues with fluorescence.

The significant difference in emission seen for nucleotides compared to the corresponding CDNs, can be exploited for monitoring the enzymatic transformations. The bacterial enzyme DncV was thus incubated with either GTP, thGTP, ^{tz}GTP or mixtures thereof under the same conditions as the HPLC-monitored reactions. Aliquots were treated with calf intestinal alkaline phosphatase (CIAP) at designated times, and emission spectra were taken after appropriate dilution (see Methods in SI for details). Rewardingly, significantly diminished fluorescence intensities were observed for the syntheses of all four homodimeric and mixed fluorescent c-di-GMP analogs, as hypothesized (Figure 5).

Unlike integrate chromatographic analyses, which can separately account for all individual species present, the observed fluorescence signal reflects the sum of all emissive species. To facilitate quantitative analyses of fluorescence data, a conversion factor (*a*) was introduced to the simulation of the fluorescence-monitored reaction kinetics. This factor bridges the integrated fluorescent spectrum and the concentration of a given chromophore at a given set of conditions and can be calculated from the integrated emission spectrum (FL_{int}) of a given chromophore with known concentration ([C]) using Eq 5. Since photophysical properties can be affected by reaction conditions, such as pH, ionic strength and temperature, *a* values are measured under identical conditions as the enzymatic reactions (see Table S1 for *a* values for all emissive CDN analogues). To compare the fluorescence- and HPLC-monitored reaction kinetics, Eq 6 was used to correlate the recorded fluorescence spectrum with the concentrations of different species in the reaction mixture. As a first attempt, the *k* values extracted from the HPLC analysis were used to fit the fluorescence data (referred to as FL Model 1).

$$FL_{int} = a[C] \quad (5)$$

$$FL_{int} = a_1[S] + a_2[I_1] + a_3[P] + a_4[I_2] \quad (6)$$

Whereas a_1 and a_3 could be successfully measured for the starting materials and final products, a_2 and a_4 are difficult to obtain, since the intermediates are produced in small quantities. We therefore first assume that $a_2 \approx a_3 \approx a_4$ in Eq 6. The calculated curve fitted well to the experimental data for c-di-^{tz}GMP synthesis with $R^2 = 0.976$, indicating excellent agreement between the reactions monitored by HPLC and fluorescence (Figure 6a). For c-di-thGMP synthesis, the observed fluorescence signal decreased faster than modeled for the first 40 minutes (Figure 6b), which resulted in a poorer fit (R^2 =0.833). In addition to the previously discussed reasons, potentially leading to poorly simulated curves for this HPLC analyzed reaction (Figure 3i), the significant accumulation of intermediates (pthGpthG or pppthGpthG) during the first 80 reaction minutes, hampers the simulation of its fluorescence response. Possible differences between the photophysical properties of the intermediates and the product are thus more influential on the analysis of c-di-thGMP synthesis as our assumption of $a_2 \approx a_3 \approx a_4$ in Eq 6 is challenged.

In addition to using chromatographically determined k values (Scheme 1a), we also simplified the analysis of the homodimeric CDNs synthesis to a pseudo-second order reaction (Scheme 1b). This approach relies on the observation that the intermediates are present in relatively low concentrations (and hence contribute less to the overall fluorescence signal). The apparent kinetics rate constant (k_{app}) was extracted with equations 7–9 (referred to as FL Model 2).

$$d[S]/dt = -2k_{app}[S]^2 \quad (7)$$

$$d[P_{app}]/dt = k_{app}[S]^2 \quad (8)$$

$$FL_{int} = a_1[S] + a_3[P_{app}] \quad (9)$$

Based on our hypothesis, k_{app} in Scheme 1b should be comparable to k_1 in Scheme 1a, as the major contributor to the change in fluorescence signal is the formation of the first intermediate (I_1). Rewardingly, using FL Model 2, the simulated curve fits well the experimental data for c-di-^{tz}GMP with R^2 =0.995, and derived k_{app}=1.57±0.15 M^{-1} s^{-1}, which is close to the k_1 derived from HPLC analysis (1.26±0.07 M^{-1} s^{-1}) (Figure 6a, Table S2). Similar to FL model 1, the simulation curve did not fit as well for the synthesis of c-di-thGMP (R^2 = 0.921, Figure 6b). The k_{app} value derived from the pseudo-second order simulation was slightly larger than the k_1 values derived from HPLC analysis (0.530±0.05 and 0.308±0.03 M^{-1} s^{-1}, respectively), but overall the two k values were still comparable (Table S3). The accumulation of intermediates during c-di-thGMP synthesis makes the simplification to a pseudo-second order reaction challenging. Adjusting the apparent rate

constant yields only minor improvement for the simulation. Nevertheless, these observations reflect our previous observations, highlighting the higher isofunctionality of the isothiazolo family of purine surrogates compared to the thiopheno family.[12d, 26]

RocR-mediated CDN hydrolysis monitored by HPLC.

Beside the cyclases that synthesize c-di-GMP, its hydrolysis to linear pGpG or GMP by PDEs is key to controlling the global and local concentration of such messengers in bacteria and hence to regulating downstream processes.[1a, 27] rocR is a PDE that contains an EAL domain and specifically recognizes and cleaves c-di-GMP into a dinucleotide monophosphate pGpG.[28] It is one of *P. aeruginosa*'s most active and well-studied PDEs.[28a, 29] To shed light on the substrate–enzyme interactions and its suitability for fluorescence monitoring, enzymatically synthesized c-di-GMP, c-di-^{tz}GMP, c-di-thGMP, c-GthGMP and c-G^{tz}GMP were incubated with rocR, and the relative concentrations of starting material (CDN) and product (pNpN) at designated time points were monitored by HPLC (Figure S6). Notably, the assigned identity of the products was confirmed by LC-ESI-TOFMS (Figure S7–S12).

RocR is reported to follow Michaelis-Menten kinetics.[27c, 28a] Scheme 2a was therefore used to analyze the reaction kinetics, where k_1 and k_{-1} describe the enzyme/substrate association and dissociation, respectively, while k_2 reflects the cleavage reaction. Equations 10–13 were thus used to extract the rate constants. When "asymmetrical" mixed c-di-GMP analogues are treated with rocR, the enzyme may, in principle, recognize and cleave either phosphodiester bonds, producing pN_1pN_2 and pN_2pN_1. Assuming the two products result from different binding orientation of the heterodimeric CDNs, Scheme 2b is therefore introduced to model the cleavage reactions, where k_1, k_{-1} and k_2 reflect the association/dissociation and cleavage of the heterodimeric CDN in one orientation (ES1), respectively, and k_3, k_{-3} and k_4 reflect the other (ES2). Equations 14–19 were used to extract the rate constants.

c-di-GMP was completely cleaved by rocR to pGpG in nearly 3 minutes with $k_1 = 3.96 \pm 0.07\ \mu M^{-1}s^{-1}$ and $k_2 = 0.76 \pm 0.03\ s^{-1}$ (Figure 7a, Table 3). Enzymatic cleavage of c-di-^{tz}GMP was slower compared to c-di-GMP, but was completed within 20 min (Figure 7b) with $k_1 = 0.043 \pm 0.02\ \mu M^{-1}s^{-1}$ and $k_2 = 0.83 \pm 0.55\ s^{-1}$ (Table 3). No cleaved c-di-thGMP was observed after 40 min of incubation with rocR (Figure 7c). The rocR-mediated cleavage of the mixed c-GthGMP yielded a single product (Figure 7d), either pGpthG or pthGpG, while two products in nearly the same amount were observed for cG^{tz}GMP (Figure S6), illustrating that both pGp^{tz}G and p^{tz}GpG were produced (Figure 7e). Overall, a gradually reduced hydrolysis rate was observed as the structures progressively deviated from the parent CDN in the order: c-di-GMP, c-di^{tz}GMP, c-G^{tz}GMP, c-GthGMP and lastly c-di-thGMP (Figure 7f).

$$d[S]/dt = -k_1[E][S] + k_{-1}[ES] \quad (10)$$

$$d[E]/dt = -k_1[E][S] + k_{-1}[ES] + k_2[ES] \quad (11)$$

$$d[P]/dt = k_2[ES] \quad (12)$$

$$d[ES]/dt = k_1[E][S] - k_{-1}[ES] - k_2[ES] \quad (13)$$

$$d[S]/dt = -k_1[E][S] + k_{-1}[ES_1] - k_3[E][S] + k_{-3}[ES_2] \quad (14)$$

$$d[P_1]/dt = k_2[ES_1] \quad (15)$$

$$d[P_2]/dt = k_4[ES_2] \quad (16)$$

$$d[E]/dt = -(k_1 + k_3)[E][S] + (k_{-1} + k_2)[ES_1] + (k_{-3} + k_4)[ES_2] \quad (17)$$

$$d[ES_1]/dt = k_1[E][S] - k_{-1}[ES_1] - k_2[ES_1] \quad (18)$$

$$d[ES_2]/dt = k_3[E][S] - k_{-3}[ES_2] - k_4[ES_2] \quad (19)$$

The observed relative rates of rocR-mediated hydrolyses of the CDN analogues indicate that the presence of a nitrogen at the purine's N-7 position on at least one nucleobase is necessary for efficient substrate recognition and cleavage. The enzyme did not produce observable amounts of cleaved c-di-thGMP products after 40 min, while the majority of c-di-^{tz}GMP was found to be cleaved within 20 min, indicating that altering both N-7 positions is likely detrimental to rocR-mediated hydrolytic cleavage. With a single N-7-containing nucleobase such as in the mixed c-GthGMP, only one phosphodiester bond is cleaved by rocR. In contrast, rocR was able to recognize the mixed c-G^{tz}GMP, where donor nitrogens are present on both nucleobases, from both orientations, leading to cleavage of either phosphodiester bond and the release of pGp^{tz}G and p^{tz}GpG (Figure 7e).

Crystal structure of rocR with a bound ligand has not yet been reported, thus systematically modified CDN analogues as studied here can illustrate the importance of the nucleobases in substrate recognition and cleavage. The structure of Ykul-bound c-di-GMP shows the amide group of the highly conserved Q16 (similar to Q161 of rocR) to be hydrogen bonded to the N-7 of the guanosine found 5' to the cleavage site[27c, 29–30]. Indeed, mutation of rocR's Q161 caused a 5-fold decrease in k_{cat}, and 2-fold increase in K_M, indicating that Q161 is involved in substrate recognition.[27c] We thus conjecture that the cleavage product of c-GthGMP is pGpthG and submit that there is little bias in rocR binding/cleaving of c-G^{tz}GMP in either orientation, as $k_1 \approx k_3$, and $k_{-1} \approx k_{-3}$ (Table 3). The difference in the final percentage of the two products P_1 (58 %) and P_2 (42 %) (Scheme 2b) might be caused by

different efficiencies for the phosphodiester bond cleavage, as k_2 (3.07 ± 0.25 s^{-1}) is much bigger than k_4 (0.34 ± 0.01s^{-1}).

Monitoring CDN hydrolysis with fluorescence.

To fluorescently monitor the rocR-mediated CDN hydrolysis, the enzymatic reactions with c-GthGMP, c-G^{tz}GMP and c-di-^{tz}GMP were executed in cuvettes under the same conditions as the reactions monitored with HPLC, and emission spectra were taken at designated time points. As shown in Figures 8 and S13, significant decrease of emission was observed during c-GthGMP and c-G^{tz}GMP hydrolysis. The fitted curves were generated with the same rate constants derived from HPLC analysis. In addition to Equations10–19, Equations 20 and 21 were used to correlate fluorescence signal with concentration for reactions described in scheme 2a and 2b, respectively.[31] The fluorescence conversion factors (*a*) are listed in Table S4. The resulting R^2 values for c-GthGMP and c-G^{tz}GMP hydrolysis monitored by fluorescence were 0.986 and 0.916, respectively. On the other hand, rocR-mediated c-di-^{tz}GMP hydrolysis did not lead to significant change in emission intensity (Figure S13c). It is possible that p^{tz}Gp^{tz}G and c-di-^{tz}GMP have similar photophysical properties, suggesting that our assumption of $a_2 \approx a_3 \approx a_4$ in Eq 6 when monitoring CDN synthesis with fluorescence stands well.

The relatively small differences in emission intensities of the CDNs and the corresponding rocR-cleaved linear products, reflects the complexity in foreseeing how changes in molecular structure impact the photophysical features. The quenching effect of fluorescent nucleosides in CDNs and their degradation products is indeed dependent on several factors associated with their building blocks, including their stacking distance and orientation, as well as their collisional dynamics and possibly aggregation. To further test the proposed model shown in Figure 1, we spectroscopically assessed the complete cycle of CDN synthesis and hydrolysis.

$$\mathrm{FL_{int}} = a_1[\mathrm{S}] + a_2[\mathrm{P}] \tag{20}$$

$$\mathrm{FL_{int}} = a_1[\mathrm{S}] + a_2([\mathrm{P_1}] + [\mathrm{P_2}]) \tag{21}$$

The fluorescent NTPs were thus incubated with DncV and quenched with CIAP at designated time points (under the same conditions as DncV-mediated synthesis above). The samples were then digested with S1 nuclease to yield the free nucleosides.[32] This hydrolysis process was monitored by fluorescence spectroscopy. Similar to the results described above, the fluorescence intensity decreased upon incubation with DncV for both ^{tz}GTP (dashed or solid black lines in Figure 9a–c) and thGTP (dashed or solid blank lines Figure 9d–f). Increasing fluorescence intensity was then observed upon administration of S1 nuclease to the DncV-mediated reaction mixtures, and the emission intensity at S1 endpoint is comparable to that of DncV at time 0 (colored lines in Figure 9), as one would predict based on the model presented in Figure 1. The same trends were observed for samples incubated with DncV for different amount of time (Figure 9c, f). The recovery of emission after S1 nuclease mediated hydrolysis reactions further supports our model, suggesting that

the fluorescence quenching observed during DncV-mediated CDN syntheses is caused by the spatial proximity of chromophores. While unlikely under our reaction conditions, intermolecular aromatic interactions could also contribute under certain circumstances, as CDNs have been reported to equilibrate between monomeric and intercalated dimeric structures.[27a]

Conclusions

Since the discovery of c-di-GMP in 1987, the landscape representing the signaling mechanisms and biological significance of CDNs has continued to expand.[1a, 5b, 27a, 33] As second messengers, the intracellular concentration of CDNs is tightly modulated by multiple dinucleotide cyclases and phosphodiesterases (PDEs), which further impact bacterial homeostasis and virulence through CDN-regulated signaling machineries, including riboswitches and protein receptors.[5b, 27a] In this study we have demonstrated the utility of novel isomorphic fluorescent analogues of this key bacterial messenger for monitoring the activity of a cyclase and both specific and non-specific phosphodiesterases in real-time. A comparison to traditional methods (e.g., HPLC) shows the fluorescence-based approach is reliable and much faster, making it amenable to further optimization and potential applications requiring higher throughput. The subtle structural differences between G and its emissive surrogates thG and ^{tz}G, provided insight into the molecular signatures governing the enzyme–substrate recognition.

Previous structural studies have illustrated that DncV belongs to a large family of nucleotidyltransferases (CD-NTases) that is responsible of synthesizing various types of CDNs as well as cyclic trinucleotides.[6] Recent reports have indicated that theses CD-NTases and their products might play distinctive roles in host-pathogen interactions, though detailed analyses are needed to further illustrate their function and signaling mechanism.[6] The isomorphic fluorescent NTPs and their CDNs described in this contribution could serve as powerful tools for the study such processes in vitro, shed light on their recognition features and accelerate the fabrication of high throughput discovery assays for agonists and antagonists.

Supplementary Material

Refer to Web version on PubMed Central for supplementary material.

Acknowledgements

We thank the National Institutes of Health for generous support (through grant GM 069773) and the Chemistry & Biochemistry MS Facility. We thank Woojoo Eunice Kim and Thomas Bartholow (Burkart lab, UCSD) for their assistance with protein expression. We are also grateful to Professor Ming C. Hammond (University of Utah) for her kind assistance in the early stages of this project.

References

[1]. a)Jenal U, Reinders A, Lori C, Nat. Rev. Microbiol 2017, 15, 271–284; [PubMed: 28163311]
b)Corrigan RM, Gründling A, Nat. Rev. Microbiol 2013, 11, 513–524. [PubMed: 23812326]
[2]. Danilchanka O, Mekalanos JJ, Cell 2013, 154, 962–970. [PubMed: 23993090]

[3]. a)Zhang X, Shi H, Wu J, Zhang X, Sun L, Chen C, Chen ZJ, Mol. Cell 2013, 51, 226–235; [PubMed: 23747010] b)Gao P, Ascano M, Wu Y, Barchet W, Gaffney Barbara L., Zillinger T, Serganov Artem A., Liu Y, Jones Roger A., Hartmann G, Tuschl T, Patel Dinshaw J., Cell 2013, 153, 1094–1107; [PubMed: 23647843] c)Chen Q, Sun L, Chen ZJ, Nat. Immunol 2016, 17, 1142–1149. [PubMed: 27648547]

[4]. McFarland AP, Luo S, Ahmed-Qadri F, Zuck M, Thayer EF, Goo YA, Hybiske K, Tong L, Woodward JJ, Immunity 2017, 46, 433–445. [PubMed: 28329705]

[5]. a)Krasteva PV, Sondermann H, Nat. Chem. Biol 2017, 13, 350–359; [PubMed: 28328921] b)Kalia D, Merey G, Nakayama S, Zheng Y, Zhou J, Luo Y, Guo M, Roembke BT, Sintim HO, Chem. Soc. Rev 2013, 42, 305–341. [PubMed: 23023210]

[6]. Whiteley AT, Eaglesham JB, de Oliveira Mann CC, Morehouse BR, Lowey B, Nieminen EA, Danilchanka O, King DS, Lee ASY, Mekalanos JJ, Kranzusch PJ, Nature 2019, 567, 194–199. [PubMed: 30787435]

[7]. a)Diner EJ, Burdette DL, Wilson SC, Monroe KM, Kellenberger CA, Hyodo M, Hayakawa Y, Hammond MC, Vance RE, Cell Rep. 2013, 3, 1355–1361; [PubMed: 23707065] b)Launer-Felty KD, Strobel SA, Nucleic Acids Res. 2018, 46, 2765–2776. [PubMed: 29514227]

[8]. Fahmi T, Port GC, Cho KH, Genes (Basel) 2017, 8, 197 doi: 110.3390/genes8080197.

[9]. Zhou J, Zheng Y, Roembke BT, Robinson Sarah M., Opoku-Temeng C, Sayre DA, Sintim HO, RSC Adv. 2017, 7, 5421–5426.

[10]. Sinkeldam RW, Greco NJ, Tor Y, Chem. Rev 2010, 110, 2579–2619. [PubMed: 20205430]

[11]. a)Shin D, Sinkeldam RW, Tor Y, J. Am. Chem. Soc 2011, 133, 14912–14915; [PubMed: 21866967] b)Rovira AR, Fin A, Tor Y, J. Am. Chem. Soc 2015, 137, 14602–14605. [PubMed: 26523462]

[12]. a)Li Y, Fin A, McCoy L, Tor Y, Angew. Chem. Int. Ed. Engl 2017, 56, 1303–1307; [PubMed: 28000329] b)McCoy LS, Shin D, Tor Y, J. Am. Chem. Soc 2014, 136, 15176–15184; [PubMed: 25255464] c)Hallé F, Fin A, Rovira AR, Tor Y, Angew. Chem. Int. Ed. Engl 2018, 57, 1087–1090; [PubMed: 29228460] d)Feldmann J, Li Y, Tor Y, Chem.: Eur. J 2019, 25, 4379–4389. [PubMed: 30648291]

[13]. Gentner M, Allan MG, Zaehringer F, Schirmer T, Grzesiek S, J. Am. Chem. Soc 2012, 134, 1019–1029. [PubMed: 22142443]

[14]. a)Luo Y, Zhou J, Watt SK, Lee VT, Dayie TK, Sintim HO, Mol. Biosyst 2012, 8, 772–728; [PubMed: 22182995] b)Shanahan CA, Gaffney BL, Jones RA, Strobel SA, J. Am. Chem. Soc 2011, 133, 15578–15592; [PubMed: 21838307] c)Shanahan CA, Strobel SA, Org. Biomol. Chem 2012, 10, 9113–9129. [PubMed: 23108253]

[15]. a)Clivio P, Coantic-Castex S, Guillaume D, Chem. Rev 2013, 113, 7354–7401; [PubMed: 23767818] b)Wang C, Sinn M, Stifel J, Heiler AC, Sommershof A, Hartig JS, J. Am. Chem. Soc 2017, 139, 16154–16160. [PubMed: 29056046]

[16]. a)Davies BW, Bogard RW, Young TS, Mekalanos JJ, Cell 2012, 149, 358–370; [PubMed: 22500802] b)Kato K, Ishii R, Hirano S, Ishitani R, Nureki O, Structure 2015, 23, 843–850; [PubMed: 25865248] c)Lv Y, Sun Q, Wang X, Lu Y, Li Y, Yuan H, Zhu J, Zhu D, Front. Microbiol 2019, 10, DOI:10.3389/fmicb.2019.02111. [PubMed: 30728810]

[17]. Kranzusch PJ, Lee ASY, Wilson SC, Solovykh MS, Vance RE, Berger JM, Doudna JA, Cell 2014, 158, 1011–1021. [PubMed: 25131990]

[18]. Ming Z, Wang W, Xie Y, Ding P, Chen Y, Jin D, Sun Y, Xia B, Yan L, Lou Z, Cell Res. 2014, 24, 1270–1273. [PubMed: 25245040]

[19]. This dephosphorylation step simplifies the HPLC analyses.

[20]. Zhu D, Wang L, Shang G, Liu X, Zhu J, Lu D, Wang L, Kan B, Zhang JR, Xiang Y, Mol. Cell 2014, 55, 931–937. [PubMed: 25201413]

[21]. Such behavior is commonly observed for consecutive reactions; See:Espenson JE, Chemical kinetics and reaction mechanisms, 2nd ed., McGraw-Hill, New York, 1995.

[22]. In all cases k1 is much smaller than k2.

[23]. Note that I1 and I2 were not experimentally differentiated in the kinetic analysis and are shown as I = I1 + I2 in Figure 3c, Figure 3f, 3i.

[24]. Hestand NJ, Spano FC, Chem. Rev 2018, 118, 7069–7163. [PubMed: 29664617]

[25]. Sholokh M, Improta R, Mori M, Sharma R, Kenfack C, Shin D, Voltz K, Stote RH, Zaporozhets OA, Botta M, Tor Y, Mély Y, Angew. Chem. Int. Ed. Engl 2016, 55, 7974–7978. [PubMed: 27273741]

[26]. Rovira AR, Fin A, Tor Y, J. Am. Chem. Soc 2017, 139, 15556–15559. [PubMed: 29043790]

[27]. a)Romling U, Galperin MY, Gomelsky M, Microbiol. Mol. Biol. Rev 2013, 77, 1–52; [PubMed: 23471616] b)Rossello J, Lima A, Gil M, Rodriguez Duarte J, Correa A, Carvalho PC, Kierbel A, Duran R, Sci. Rep 2017, 7, DOI: 10.1038/s41598-41017-09926-41593; [PubMed: 28127057] c)Rao F, Yang Y, Qi Y, Liang ZX, J. Bacteriol 2008, 190, 3622–3631. [PubMed: 18344366]

[28]. a)Zheng Y, Tsuji G, Opoku-Temeng C, Sintim HO, Chem. Sci 2016, 7, 6238–6244; [PubMed: 30034764] b)Schmidt AJ, Ryjenkov DA, Gomelsky M, J. Bacteriol 2005, 187, 477–481.

[29]. Chen MW, Kotaka M, Vonrhein C, Bricogne G, Rao F, Chuah ML, Svergun D, Schneider G, Liang ZX, Lescar J, J. Bacteriol 2012, 194, 4837–4846. [PubMed: 22753070]

[30]. Minasov G, Padavattan S, Shuvalova L, Brunzelle JS, Miller DJ, Basle A, Massa C, Collart FR, Schirmer T, Anderson WF, J. Biol. Chem 2009, 284, 13174–13184. [PubMed: 19244251]

[31]. We assumed that P1 and P2 in Scheme 2b has similar a values.

[32]. CIAP was still in the reaction mixture, therefore all the terminal phosphate groups will be removed and leaves free nucleosides instead of nucleoside monophosphates.

[33]. a)Libanova R, Becker PD, Guzman CA, Microb. Biotechnol 2012, 5, 168–176; [PubMed: 21958423] b)Ross P, Weinhouse H, Aloni Y, Michaeli D, Weinberger-Ohana P, Mayer R, Braun S, de Vroom E, van der Marel GA, van Boom JH, Benziman M, Nature 1987, 325, 279–281. [PubMed: 18990795]

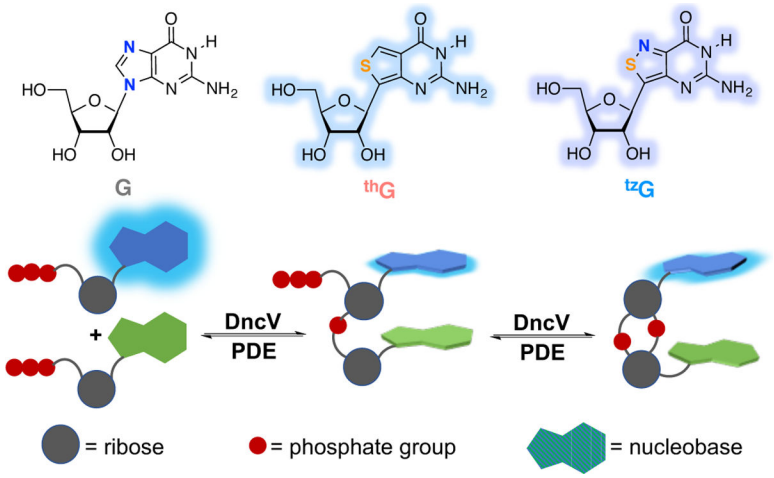

Figure 1.

Top: Guanosine and its emissive surrogates thG and ^{tz}G; **Bottom:** a hypothetical model predicting fluorescence changes upon CDN formation and hydrolysis.

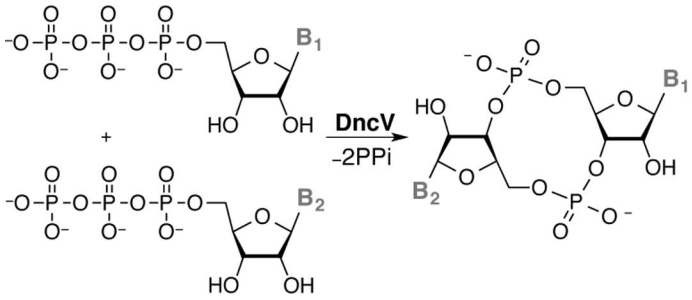

Figure 2.

Structures of the enzymatically synthesized c-di-GMP analogues. DncV is able to convert two NTPs into the corresponding homo- and heterocyclic dinucleotides. B_1, B_2 stand for nucleobases.

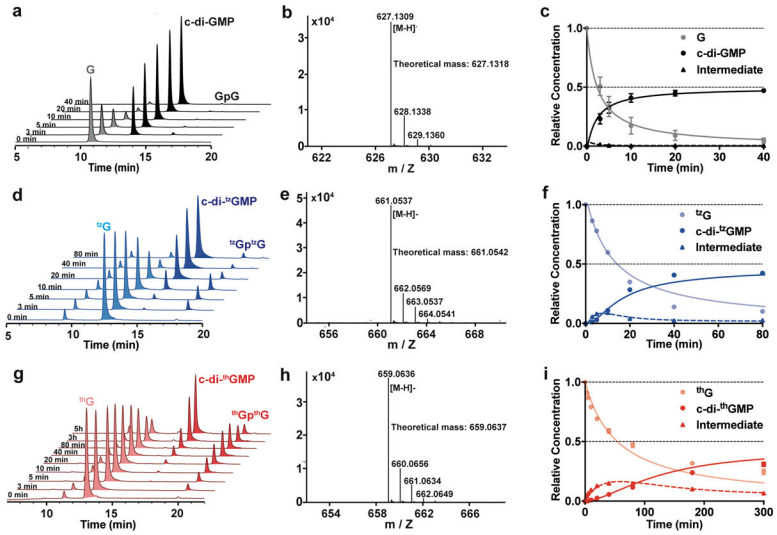

Figure 3.

DncV-mediated enzymatic synthesis of c-di-GMP and its analogues c-di-^{tz}GMP and c-di-thGMP. (a) UV-monitored HPLC chromatograms (260 nm) of the DncV-mediated synthesis of c-di-GMP; (b) HR-MS of the intermediates from CIAP-treated reaction; (c) Kinetic analysis of the HPLC-integrated relative concentration and fitted curve of the starting materials (measured as nucleosides), products and intermediates for the DncV-mediated reactions of GTP; (d)–(f) HPLC chromatograms (333 nm), HR-MS of the intermediate, and kinetic analysis of DncV-mediated synthesis of c-di-^{tz}GMP; (g)–(i) HPLC chromatograms (321 nm), HR-MS of the intermediate, and kinetic analysis of DncV-mediated synthesis of c-di-thGMP. Aliquots were treated with calf intestinal alkaline phosphatase (CIAP) at designated times, therefore the starting materials were presented as G, ^{tz}G and thG, and intermediates were presented as GpG, ^{tz}Gp^{tz}G and thGpthG. Assays were done in duplicates. Error bars indicate standard deviation (SD).

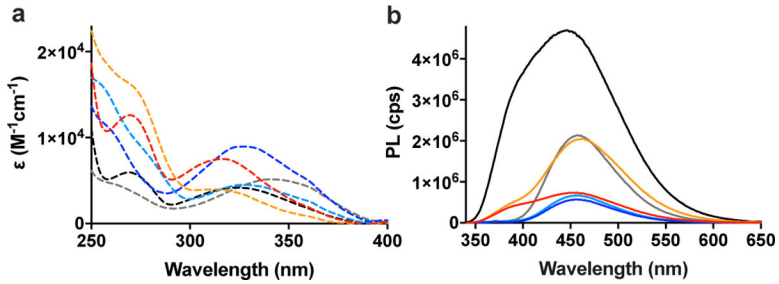

Figure 4.

Absorption spectra (a) and emission spectra (b) of thG (black), ^{tz}G (grey), c-di-thGMP (red), c-di-^{tz}GMP (indigo), c-GthGMP (orange) c-G^{tz}GMP (light blue) dissolved in water. The emission spectra were normalized to optical density of 0.1 at the excitation wavelengths (320 and 330 nm for species containing thG and ^{tz}G, respectively).

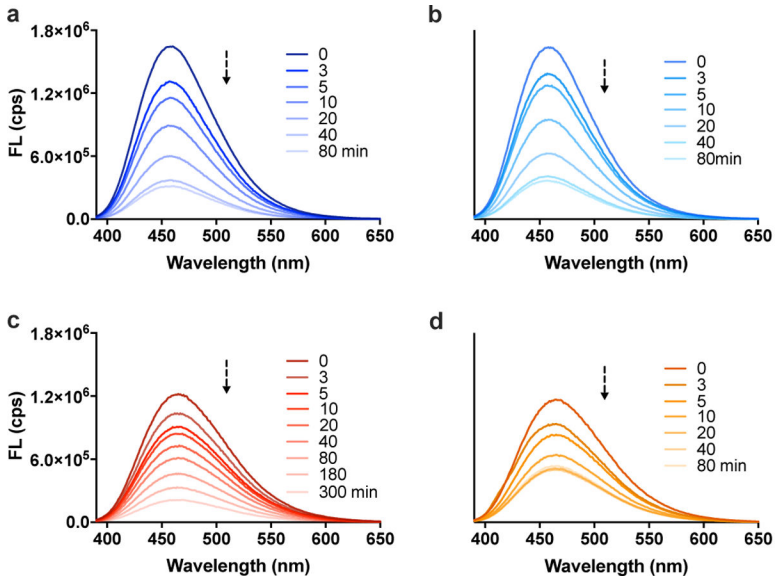

Figure 5.

DncV-mediated cyclization monitored by emission spectra for (a) c-di-^{tz}GMP, (b) c-G^{tz}GMP, (c) c-di-thGMP and (d) c-GthGMP. Excitation wavelength was 380 nm for all emission spectra.

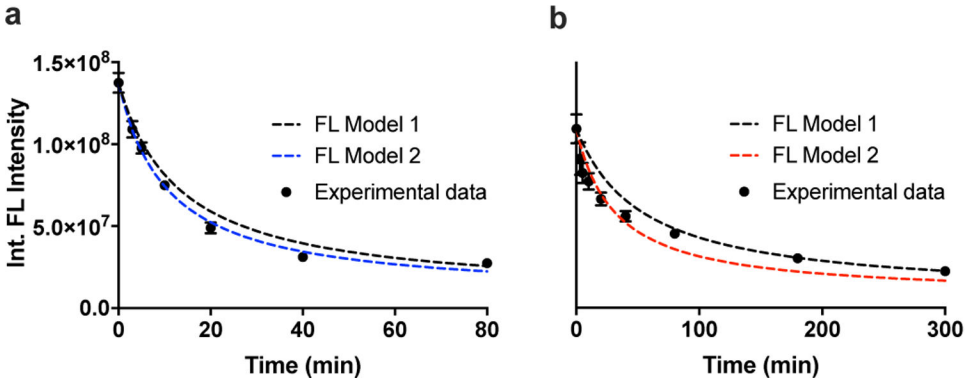

Figure 6.

Kinetics analysis of DncV-mediated synthesis of (a) c-di-^{tz}GMP (R^2 = 0.9759, 0.995 for FL model 1 and FL model 2, respectively) and (b) c-dithGMP (R^2 = 0.8325, 0.9205 for FL model 1 and FL model 2, respectively).

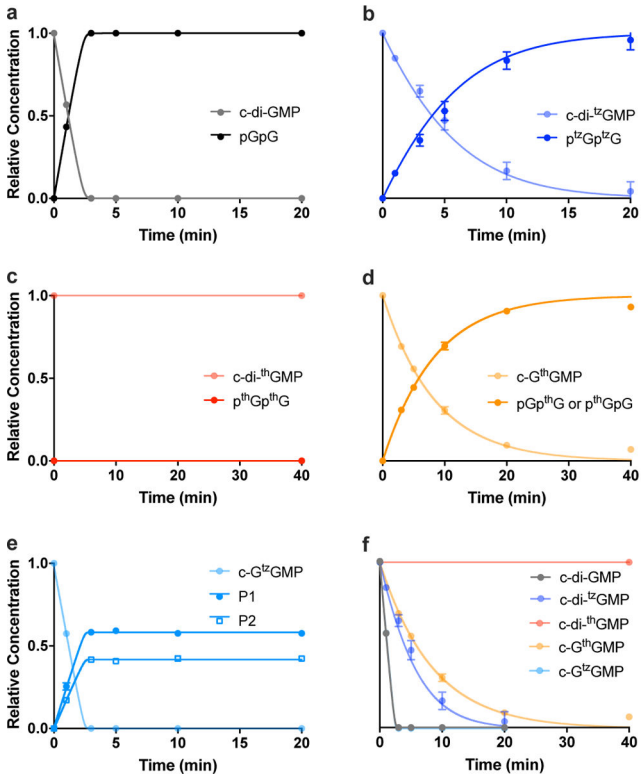

Figure 7.

Kinetics analyses of rocR-mediated cleavage of c-di-GMP analogues. The enzyme (100 nM) was incubated with 10 μM of (a) c-di-GMP, (b) c-di-^{tz}GMP, (c) c-di-thGMP, (d) c-GthGMP and (e) c-G^{tz}GMP and the reactions were quenched using 100 mM $CaCl_2$ at designated time point and analyzed by HPLC. Assays were done in duplicates. Error bars indicate SD.

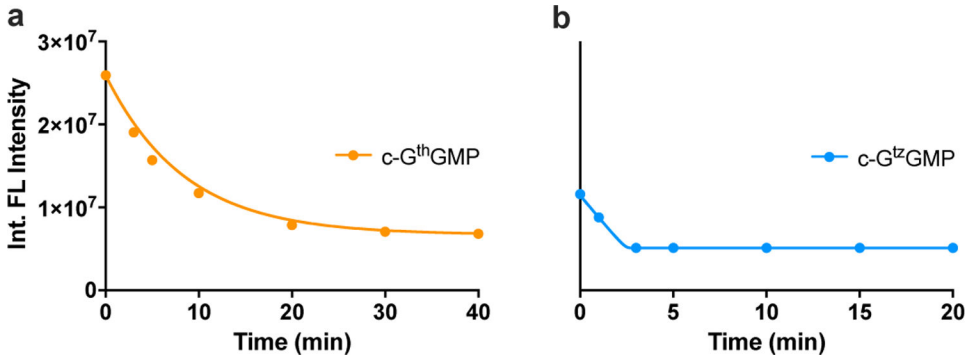

Figure 8.

rocR-mediated CDN hydrolysis monitored with fluorescence. a) rocR-mediated c-GthGMP hydrolysis monitored with steady-state emission spectra. b) rocR-mediated c-G^{tz}GMP hydrolysis monitored with steady-state emission spectra. The y-scale was integrated emission intensity (area under the curve). Assays were done in triplicates or duplicates (error bars, indicating SD, were smaller than the points shown).

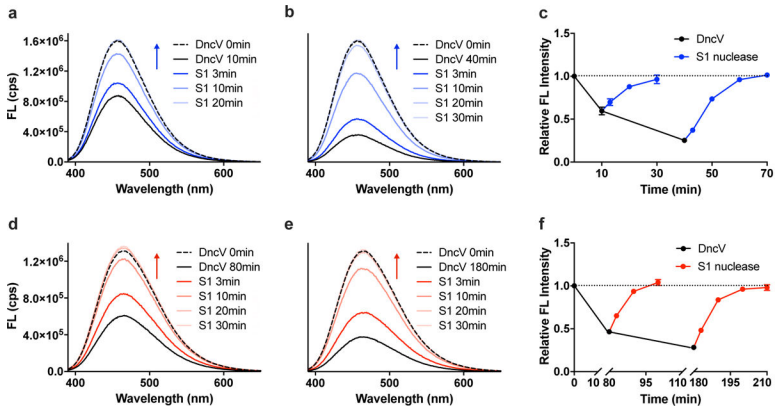

Figure 9.

DncV-mediated synthesis and S1 nuclease-mediated hydrolysis of CDNs monitored with emission spectra.

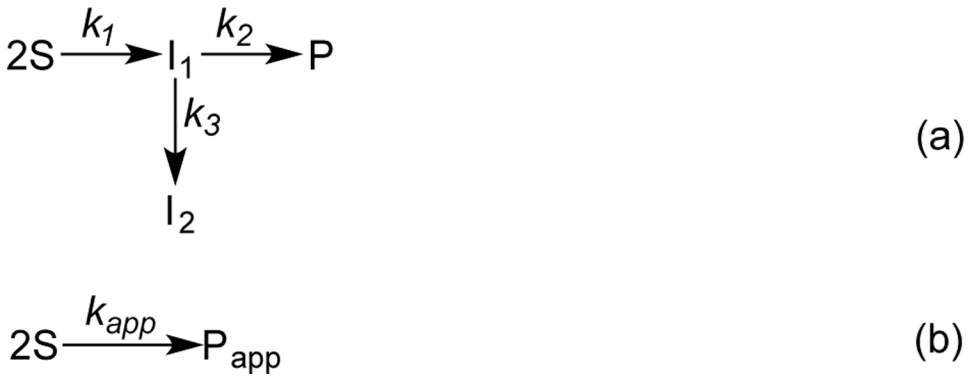

Scheme 1.

Kinetics schemes for DncV-mediated CDN synthesis. S represents the starting NTP, I_1 and I_2 respectively represent intermediates pppNpN and degraded intermediate pNpN (I= I_1 + I_2), and P represents the product CDN. P_{app} (apparent product) stands for the sum of all the dinucleotide species, including linear ones and cyclized products.

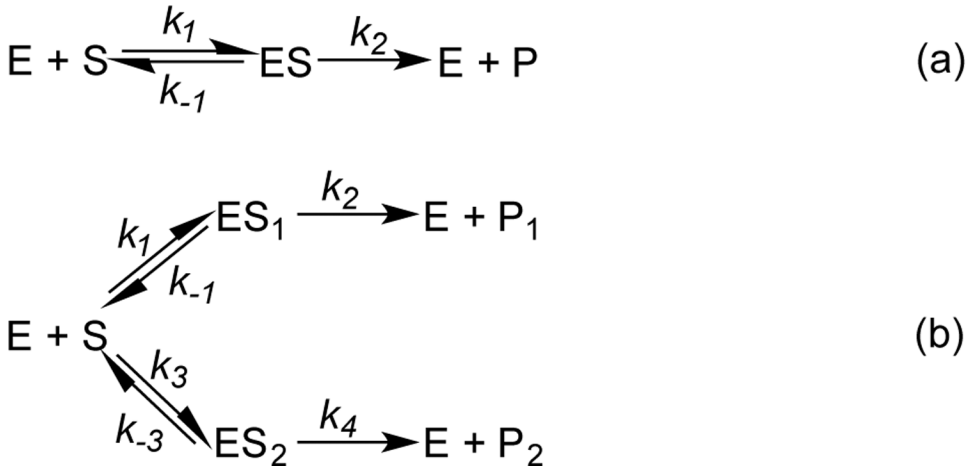

Scheme 2.

Kinetics scheme of rocR-mediated hydrolysis of CDNs. E stands for the enzyme S stands for the starting CDN, and P stands for the product. (a) Kinetics scheme of rocR-mediated hydrolysis of c-di-GMP, c-di-^{tz}GMP and c-di-thGMP. (b) Kinetics scheme of rocR-mediated hydrolysis of mixed analogues, including c-G^{tz}GMP and c-GthGMP.

Table 1.

Reaction rate constants of DncV-mediated CDN syntheses[a]

	k_1 ($\mu M^{-1}S^{-1}$)	k_2 (s^{-1})	k_3 (s^{-1})
c-di-GMP	(7.1 ±2.3) $\times 10^{-6}$	(7.4±2.1) $\times 10^{-2}$	(6.4±0.3) $\times 10^{-4}$
c-di-^{tz}GMP	(1.26±0.07) $\times 10^{-6}$	(3.4±0.2) $\times 10^{-3}$	(1.3±0.1) $\times 10^{-4}$
c-di-thGMP	(3.08±0.03) $\times 10^{-7}$	(2.32±0.05) $\times 10^{-4}$	(2.91±0.01) $\times 10^{-5}$

[a]Data were presented as mean ± SD. See Methods in SI for details.

Table 2.

Photophysical properties of emissive nucleosides and CDN analogues[a]

	λ_{abs}^{max} (nm)	ε (M^{-1} cm^{-1})	λ_{em}^{max} (nm)	ϕ	ϕ_e
thGM[a]	321	4.15×10^3	453	4.6×10^{-1}	1909
^{tz}G[a]	333	4.87×10^3	459	2.5×10^{-1}	1203
c-di-thGMP	317	7.47×10^3	457	7.7×10^{-2}	575
c-di-^{tz}GMP	331	8.77×10^3	456	3.9×10^{-2}	342
c-GthGMP	317	3.54×10^3	458	1.8×10^{-1}	636
c-G^{tz}GMP	331	4.38×10^3	456	4.8×10^{-2}	210

[a]Values for thG and ^{tz}G were obtained from previous publications.[11]

Table 3.

Reaction rate constants for rocR-mediated CDNs cleavage[a]

	k_1 ($\mu M^{-1}s^{-1}$)	k_{-1} (s^{-1})	k_2 (s^{-1})	k_3 ($\mu M^{-1}s^{-1}$)	k_{-3} (s^{-1})	k_4 (s^{-1})
c-di-GMP	3.96 ± 0.07	1.15 ± 0.21	0.76 ± 0.03	NA	NA	NA
c-di-^{tz}GMP	0.043 ± 0.02	0.09n± 0.07	0.83 ± 0.55	NA	NA	NA
c-GthGMP	0.021 ± 0.001	0.033 ± 0.001	5 ± 0.57	NA	NA	NA
c-G^{tz}GMP	1.85 ± 0.07	0.096 ± 0.091	3.07 ± 0.25	1.8 ± 0.1	0.135 ± 0.007	0.34 ± 0.01

[a]Data were presented as mean ± SD.